Rock Mechanics
and Rock Engineering 25, 109—140

Rock Mechanics and Rock Engineering

Size and Shape Effects in Point Load Tests of Irregular Rock Fragments

By

L. A. Panek[1] and **T. A. Fannon**[2]

[1] Formerly J. S. Westwater Professor of Mining Engineering
[2] Formerly Graduate Student, Mining Engineering
Michigan Technological University, Houghton, Michigan, U. S. A.

Summary

Point-load tests were performed on three hard rocks of the Lake Superior district, ironformation, metadiabase, and ophitic basalt. More than 500 irregular, mine-run fragments ranging in diameter up to about 250 mm were tested in the field, using a specially designed, semi-portable test rig. Results were analyzed by multiple regression techniques, seeking a "best" expression for the point-load strength in terms of a size effect and shape effects. Standard unconfined compression tests and "Brazilian" tests were also performed on the metadiabase and the basalt, three core sizes of each, in order to determine their respective size effects. The size-effect exponents for compression were found to be a variable characteristic of rock type, as previously reported for other rocks by the senior author, whereas the size-effect exponent in the point-load test was constant over all three rocks.

Notation

A	Load-bearing area of prismatic compression specimen, mm^2
α	Probability level of a statistical significance test
b, w	Long and short prism dimensions, mm, in plane perpendicular to load
c_I, c_L	Exponent in equation for strength (coefficient, in the log-linear form)
d	Diameter, mm
D, H	Initial and final (at rupture) distance between the load points, mm
E	Young's modulus, MPa
F	Axis of the fracture surface normal to D, mm, point-load test
G, J	Semiminor, semimajor, specimen axis, mm, perpendicular to direction of point load
h	Height of prismatic compression specimen, mm
K	Constant in linear regression model, basic rock strength parameter
L, M, S	Long, intermediate, and short axes, of point-load-test specimen

log	Natural (Napierian) logarithm
n	Number of tests
v	Poisson's ratio
P	Resistance of test specimen at rupture, Newtons
Q	Compressive strength, MPa, determined from unconfined compression test
R	Multiple correlation ratio for a multilinear regression analysis
SE	Standard error of estimate for a multilinear regression analysis
T	Tensile strength, MPa, determined from diametral compressive test of core
t	Thickness, mm
U	Geometric mean diameter, mm, of the minimum cross section through the load points $= (DG)^{1/2}$
V	Geometric mean diameter, mm, of point-load specimen $= (LMS)^{1/3}$
W	Geometric mean diameter, mm, of the specimen midsection perpendicular to the point-load direction $= (GJ)^{1/2}$
X, Y	Geometric mean diameter, mm, of the fracture surface, estimated by $(DF)^{1/2}$, by $(HF)^{1/2}$
$Z_{LM}, Z_{RA}, \ldots$	Differences between values of log K, used to express category effects, those attributed to specimen orientation and/or rock type

1. Introduction

Rock testing can become more widely performed and thus much more useful if schemes can be developed to reduce the time and expense entailed. Point-load testing of irregular rock fragments appears to be an attractive approach. To this end, the senior author devised a semiportable apparatus for performing point-load-strength tests of irregular fragments up to about 270 mm diameter, so that fragments could be tested where found, e. g. at virtually any location in a mine, and tests of a range of sizes would yield estimates of the strength-size effect, as well as the strength of the rock. To enhance the generality of conclusions from the tests analyzed herein, three different rock types were tested. To relate the PL (point load) test results to more conventional rock test values, core specimens of two of the rocks were prepared in three different diameters and subjected to standard unconfined compression (UC) tests and diametral compressive (DC) load ("Brazilian") tests, since brittle fracture appears to be initiated by a splitting process in all three test methods.

Numerous investigators have contributed to our knowledge of various aspects of PL testing during the past three decades. Protodyakonov and Voblikov (1957) and colleagues seem to have been the earliest to pursue systematically the testing of irregular specimens of rock, crushing them between two flat-surface platens. The paper by Broch and Franklin (1972), which popularized the point-load testing of drill cores, contains an extensive review of the topic. The ISRM commissions on testing methods (1972 and 1985) issued recommended procedures for point-load testing. The

point-load test, generally regarded as an index test, has more recently been used to estimate the "uniaxial" or unconfined compressive strength of rock. By far the greatest attention has been given to tests of specimens created by core drilling, which has only limited relevance to the present investigation. Also, past testing has been narrowly focused, especially in the analysis of the data, investigating the influence of one variable at a time. The revised recommended method for PL testing (ISRM, 1985) reflects repeated proposals to improve the method of calculating the PL strength index. The present investigation, however, is not particularly oriented toward a standard testing procedure; standardization inevitably tends to hinder the search for broader understanding. Rather, the objective is to determine the influences of specimen size and shape on the point-load strength of rock fragments, not by theoretical analysis of any idealized specimen, but rather by multivariate analyses of tests performed along the three major axes of irregular specimens, as best these can be determined rapidly under field conditions.

2. Rock Specimens

The three rock types tested are crystalline rocks of middle Precambrian age, about one billion years old, from iron and copper mines of the Lake Superior district. Choice was based primarily on the ready availability of sufficient quantities of uniform materials. Attempt was made to test the rock as nearly as possible in its natural moisture and temperature condition. This is easily achieved for the PL tests of irregular fragments, which are essentially tested on site with the semi-portable test rig. However, maintaining the natural moisture condition of laboratory UC and DC test specimens is questionable, in view of their being prepared by diamond drilling and surface grinding. These were nevertheless stored in plastic trash bags; cumulative exposure to the laboratory atmosphere during specimen preparation was one to two days between drilling and testing. At the start of the laboratory test period for each rock type, weight measurements indicated a free water content of 1.3% for the basalt one week after drilling, and 0.12% for the metadiabase one month after drilling (one year after blasting).

Iron-formation and metadiabase were obtained from the Tilden Mine, an open pit operated near Ishpeming, Michigan, by Cleveland Cliffs Iron Company. Iron-formation refers herein to a banded rock, comprised essentially of recrystallized martite and chert in roughly equal proportions. The iron-oxide grains range in size mostly between 10 and 25 microns (Villar and Dawe, 1975). Run-of-mine fragments of iron-formation, obtained (following the removal of blasted ore) from the sloughed back-break of a blast executed 10 weeks earlier, were selected in August 1987 to cover the range of sizes that could be tested in the PL tester. Some of the fragments were tested at the mine for one day; to save the 290-km round trips, the remainder was tested out of doors within the next two days at MTU. The PL specimens were tested under overcast sky, at air temperature 20 °C.

The metadiabase was one of several dikes that intrude the Tilden ore body. Thin sections revealed low-grade, greenschist-facies metamorphism (W. I. Rose, personal communication, February 1989), with incomplete and variable recrystallization, leaving small (< 1 mm) secondary crystals within the relict boundaries of the larger (3—6 mm) primary crystals. For PL testing, irregular run-of-mine fragments, obtained from the sloughed backbreak of a blast 10 weeks earlier, were selected from 60 m of the 90 m of exposed length of the dike on the mining bench. Most of the PL specimens were tested out of doors at the Tilden Mine in August and October 1987 or at MTU in August, under overcast sky or shaded from direct sunlight or in the evening, with air temperature in the range 10—22 °C; the last 6 specimens were tested in December, the fragments having been stored in the open air of MTU Experimental Mine (high humidity, temperature 10 °C) to prevent their drying out. Most of the core (three diameters, 28, 51, and 145 mm) for the UC and DC tests was diamond-core drilled from four large blocks obtained from a 3-m length of exposure at the east end of the 90-m sampling section. Although core runs were not referenced to their parent blocks, a small block taken from the west end of the sampling section yielded only a single run of 145-mm-diam core. Core recovery was 100%.

Basalt rock was obtained from the MTU Experimental Mine, essentially a 600-m-long footwall adit connection to the Quincy Mine, no longer operating, which produced native copper for many years. Rock exposed in the adit consists almost entirely of a succession of basaltic lava flows, conformably dipping about 55°, a section of the Portage Lake Lava Series, which has total thickness of at least 5000 m. Petrographically, the rock is ophitic basalt, consisting essentially of augite crystals (up to 8 mm) enclosing laths of (1—2 mm) labradorite. The sampling site is 128 m below surface and free from obvious jointing. Core for UC and DC specimens was produced by diamond drilling 6 parallel holes (two each of core diameters 21 mm, 70 mm, and 145 mm) about 60° to the strike direction, collared within a rectangle 0.3 m by 0.4 m. The smaller holes were drilled to 1.5 m depth, the 145-mm holes to 3 m. Core recovery was 100%. Rock material was several times blasted off the adjacent 7.6 m length of exposed drift wall to produce fragments for PL tests. The selected fragments were tested in the mine (air temperature 10 °C, approximately the rock temperature).

3. Unconfined Compression (UC) Tests

Test Procedure

In all, 40 cylindrical specimens of metadiabase and 44 of basalt, each rock type represented by three core sizes, were tested to rupture in a computer-controlled, servohydraulic, ultra-stiff, 5-MN-capacity load frame. All specimens were prepared according to standard specifications for UC tests, with ends ground parallel, flat, and perpendicular to the cylinder axis. All had

the same shape, height/diameter $\cong 2$; this ratio is in the range where minor variations in the ratio have little effect on specimen strength.

Loads were transmitted to the specimens through flat-surface, hardened steel platens having diameters the same as the test specimens, which commonly has been found to minimize end restraint. Load was increased at a linear rate to failure; the load rates were in the range 0.13 to 0.55 MPa/s, which approximate the rates recommended by ISRM and ASTM. During tests of basalt, axial and circumferential strains were measured with 25-mm-gage-length extensometers; because of difficulties with the latter, v (mean value 0.20) was determined only from the first three tests. For tests of metadiabase, bonded foil-type electric-resistance strain gages (gage length 6—9 mm) were substituted for one or both extensometers (mean $v = 0.26$ from 29 determinations). For both rock types, the recordings of load vs. strain showed approximately linear stress-strain behavior up to rupture. Brittle extension fractures dominated (longitudinal splitting), Fig. 1, with minor shearing on inclined surfaces; very few cone-shaped end pieces were produced. Post-peak behavior could not be observed, because of the programed uniform rate of load increase.

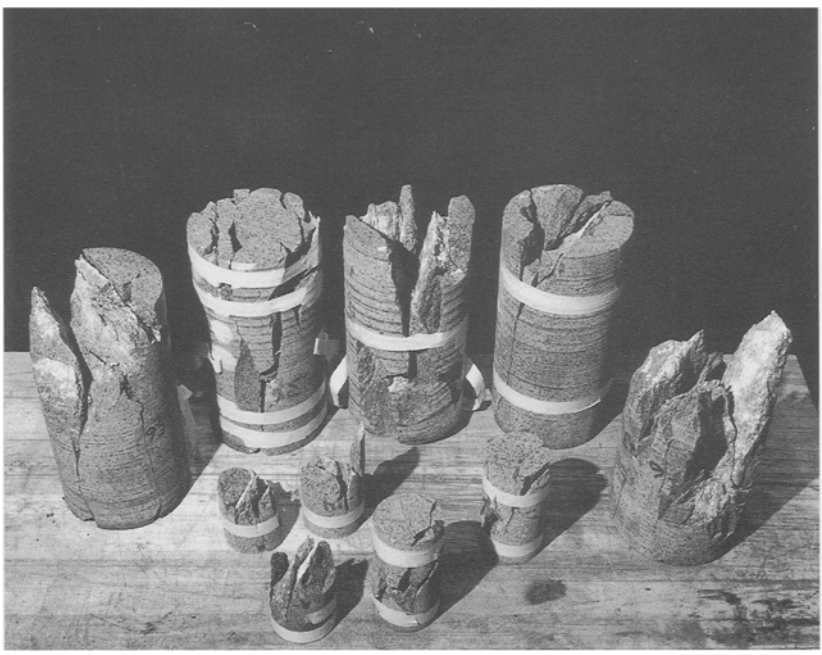

Fig. 1. UC tests-fractured specimens 70 and 145 mm diam.

Rationale of Analysis

Unconfined compressive strength tests of prismatic specimens of brittle rocks and coals made by many investigators have shown (Panek, 1981) that

the compressive stength Q calculated from the conventional formula $Q = P/A$ can be expressed in the form

$$Q = K_1 (1/w)^{c_1} (w/h)^{c_2} (b/w)^{c_3}, \tag{1}$$

where K_1 is a parameter reflecting the basic strength of the material, $(1/w)^{c_1}$ is the strength-size effect, $(w/h)^{c_2}$ is a shape effect, and $(b/w)^{c_3}$ is another shape effect. The size-effect exponent c_1, interpreted to be a material characteristic, was found to range in value from 0 to 0.5, taking a value about 0.07 for fine-grained sedimentary rocks, about 0.22 for granitic rocks, and 0.12 to 0.50 for coal seams ranging in character from massive to friable. Shape-effect exponents were found to be $c_2 \cong (c_1 + 1/3)$ and $c_3 \cong 0.1$.

The parameter K_1 necessarily includes the effects of all factors that do not appear in Eq. (1), such as the friction on the end surfaces and the moduli of the specimens and the load platens. For example, if the test specimens are cylindrical ($w = b = d$) and all of the same shape, but of assorted sizes, then w/h and b/w are constant in the experimental data, which can be analyzed only for the size effect, the objective of the present investigation, using the reduced model

$$Q = K_2 (1/d)^{c_1}. \tag{2}$$

Unconfined Compressive Strength — Analysis of Data

For each test, the compressive strength was calculated from $Q = P/A$. E was calculated as the two-point tangent modulus from $0.1P$ to $0.6P$, approximately. Values of K_2 and c_1 were obtained by standard regression analysis of the following model, the linearized form of Eq. (2):

$$\log Q = \log K_2 + c_1 (\log 1/d) \tag{3}$$

Results are summarized in Table 1.

Table 1. Unconfined compression (UC) tests

	Metadiabase			Basalt		
Diameter of core (d), mm	28	51	145	21	70	145
Number of tests	14	18	8	27	9	8
Mean value of Q, MPa	239	185	128	191	171	161
Standard deviation of Q, MPa	35.6	62.1	27.4	17.1	19.9	31.0
Mean value of E, GPa	78.0	77.9	84.4	64.3	71.0	75.6
Standard deviation of E, GPa	6.40	8.48	5.36	5.59	9.46	4.11

A least-squares fit to the 40 tests of metadiabase yields the following:

$$\log Q = \underset{(0.294)}{6.734} + \underset{(0.074)}{0.390} \log (1/d), \quad SE = 0.273, \quad R^2 = 0.422. \tag{4}$$

(standard deviation of parameters above)

The size-effect exponent c_1 is thus 0.39 for metadiabase in compression.

A least-squares fit to the 44 tests of basalt yields the following:

$$\log Q = \underset{(0.090)}{5.551} + \underset{(0.024)}{0.098} \log (1/d), \quad SE = 0.125, \quad R^2 = 0.286. \tag{5}$$

The size-effect exponent c_1 is thus 0.10 for basalt in compression. The least-squares fits can be evaluated by examining the residuals. Residual = (Value of log Q determined by test) — (Value of log Q estimated by the least-squares solution). The residuals with respect to log Q values estimated for the test specimens by Eqs. (4) and (5) are plotted in Fig. 2.

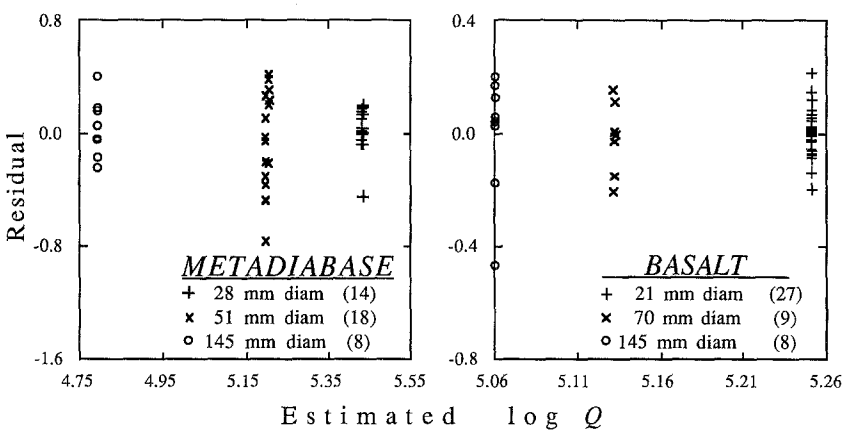

Fig. 2. Unconfined compression tests, residuals with respect to fitted Eqs. (4) and (5)

4. Diametral Compressive (D C) or Brazilian Tests

Test Procedure

Test specimens, thickness/diameter = 1/2, were prepared from cores of metadiabase and basalt in three different diameters each. Fewer 70-mm-diam basalt specimens were produced than planned, because of damage to the core barrel. The larger basalt specimens (70 mm and 145 mm) were found to have irregular cylindrical surfaces, and hence, in order to facilitate uniformly distributed line loading, either two diametrically opposed flats were created with a surface grinder or the cylindrical surfaces over two diametrically opposed 30° arcs were made straight by lapping.

The specimens were loaded through hardened steel platens at the rate of 0.05 to 0.10 MPa/s, approximately the ISRM/ASTM recommended rates, to determine the resistance (P) at rupture. Direction of loading was random with respect to original field orientation. Most specimens were loaded above by a flat steel platen and below by a cylindrical platen; the exceptions were the basalt specimens having diametrically opposite flats, which were loaded above and below with cylindrical platens in order to achieve the desired line loads across the thickness of the disk. The ratio of cylindrical platen diameter to specimen diameter was 0.46, 0.36, and 0.18,

respectively, for the 21-mm, 70-mm, and 145-mm basalt specimens; the ratio was 0.22, 0.25, and 0.26 for the 28-mm, 51-mm, and 145-mm metadiabase specimens.

An extension fracture usually occurred, Fig. 3, cleaving the specimen into two hemicylinders, herein designated the "classical" fracture. Very minor crushing, forming a wedge of crushed rock, commonly occurred at one platen-rock contact. In addition, a number of specimens exhibited a planar fracture that deviated noticeably, being displaced from and/or inclined to, the diametral plane through the platen contact lines, and usually not intersecting the platen contact line. Such a deviated planar fracture occurred in roughly one-half of the larger metadiabase specimens (one of the 28-mm-diam, 13 of the 51-mm-diam, and 7 of the 145-mm-diam) and roughly one-third of the larger basalt specimens (one of the 21-mm-diam, two of the 70-mm-diam, and 7 of the 145-mm-diam).

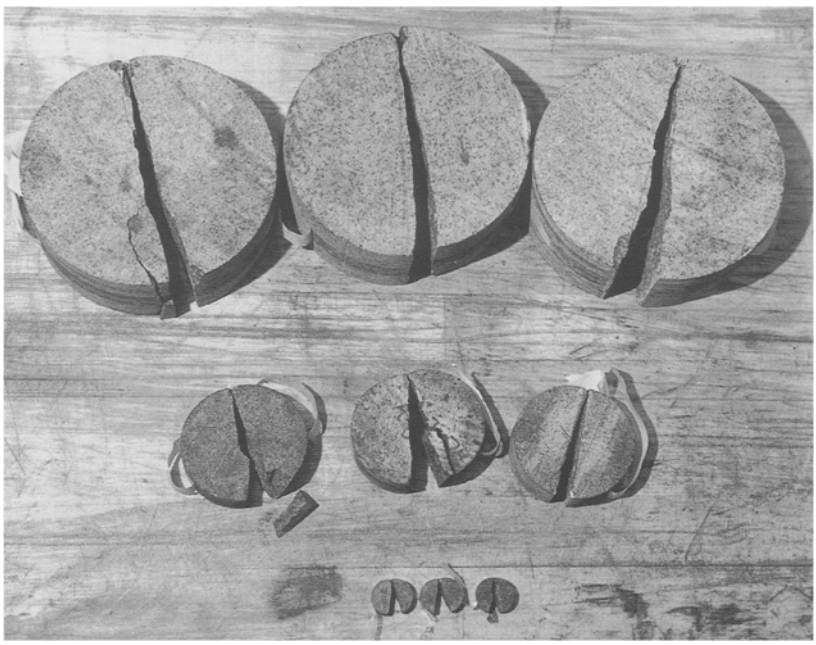

Fig. 3. DC tests-fractured specimens 21, 70 and 145 mm diam.

Rationale of Analysis

Following the approach employed to represent compressive strength as the product of powers of dimensions of the test specimens, the tensile strength T determined from diametral compressive tests similarly can be expressed as a function of a shape effect and a size effect, which, when specimen shape is constant, reduces to the strength-size relationship

$$T = K_3 (1/d)^{c_1}. \tag{6}$$

Diametral Compressive Tests — Analysis of Data

For each test the tensile strength was calculated by the conventional formula $T = 2P/\pi dt$. Values of K_3 and c_1 were obtained by standard regression analysis of the following model, the linearized form of Eq. (6):

$$\log T = \log K_3 + c_1 (\log 1/d). \tag{7}$$

In six metadiabase specimens the deviated planar fracture was the primary fracture (the classical fracture being absent), causing below-average strength values. Regression analyses identified these 6 tests as "outliers", and hence they are excluded from the results, which are summarized in Table 2. Since the basalt specimens did not exhibit instances in which the planar deviated fracture was the primary fracture, none of the basalt results are excluded, even though two tests gave borderline low strengths.

Table 2. Diametral compression (DC) tests

	Metadiabase			Basalt		
Diameter of core (d), mm	28	51	145	21	70	145
Number of acceptable tests	22	24	12	14	6	26
Mean value of T, MPa	19.3	17.0	13.4	15.7	9.11	9.00
Standard deviation of T, MPa	2.19	2.27	1.74	1.14	1.02	1.21

A least-squares fit to the 58 tests of metadiabase yields the following:

$$\log T = \underset{(0.113)}{3.697} + \underset{(0.028)}{0.222} \log (1/d), \quad SE = 0.130, \quad R^2 = 0.522. \tag{8}$$

The size-effect exponent c_1 is thus 0.22 for metadiabase in tension, as determined by DC tests. However, if none of the low strength values were excluded, c_1 would be 0.32; if only the two lowest were excluded, c_1 would be 0.26; and if only the four lowest were excluded, c_1 would be 0.22, the same as Eq. (8), apparently a stable value. Rejection of test data clearly introduces some uncertainty into the interpretation.

A least-squares fit to the 46 tests of basalt yields the following:

$$\log T = \underset{(0.104)}{3.614} + \underset{(0.024)}{0.292} \log (1/d), \quad SE = 0.139, \quad R^2 = 0.772. \tag{9}$$

The size-effect exponent c_1 is thus 0.29 for basalt in tension, as found by the DC test. The residuals with respect to $\log T$ values estimated by Eqs. (8) and (9) are plotted in Fig. 4.

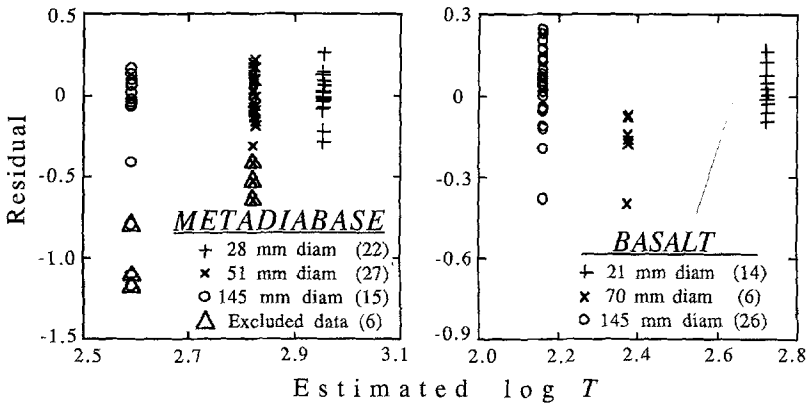

Fig. 4. Diametral compressive (Brazilian) tests, residuals with respect to fitted Eqs. (8) and (9)

5. Point Load (PL) Tests of Irregular Fragments

Test Procedure

PL tests were performed with a large, semi-portable apparatus designed by the senior author, which can accept specimens up to about 270 mm diam, Fig. 5. Load up to 200 kN is applied by a hydraulic cylinder, pressure being generated by a hydraulic hand pump. The rate of load increase during a

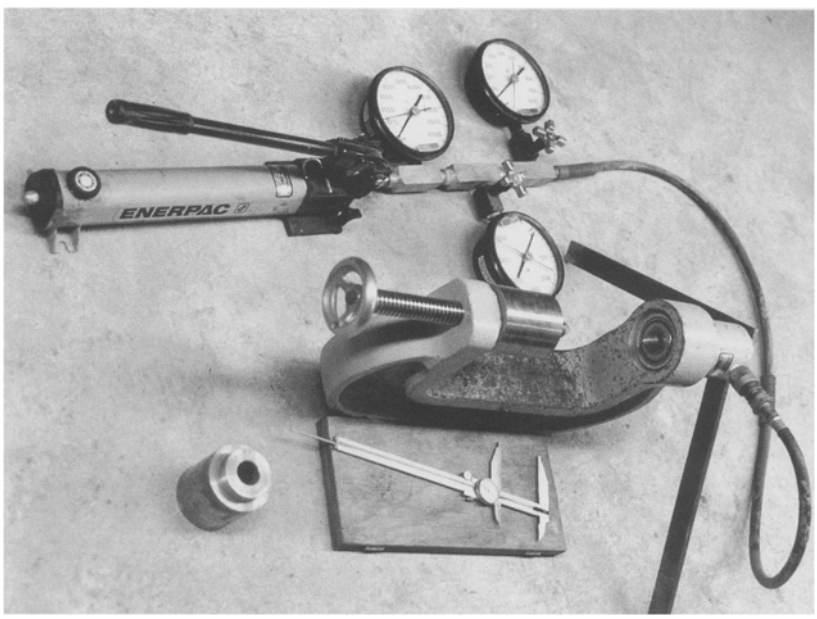

Fig. 5. Point load test apparatus

test was on the order of 0.15 kN/s. Maximum specimen resistance was indicated by a hydraulic gage, of which three were connected, with ranges 0—7, 0—20, and 0—69 MPa. The apparatus was calibrated (for each hydraulic gage) by pumping (expanding) the hydraulic cylinder against the platens of a laboratory load frame, itself annually calibrated to within 1% accuracy, to determine the equation for force applied by the cylinder as function of the hydraulic gage reading.

Load platens for the PL tests in most instances were the usual 60° cones with 5-mm-radius tip (ISRM, 1972 and 1985), made of hardened steel. Because prior experience with the device had shown a tendency for a cone platen to slide down-slope when the load has to be applied non-normal to the surface of an irregular rock fragment, cylindrical platens 28 mm diam (the contact surface) by 25 mm long were also provided, whereby the flat surface of the platen applied the load to an edge or vertex of a difficult specimen. Note was made of tests that used such flat-surface platen(s).

The dimensions of an irregular fragment are taken to be the lengths L, M, and S of the long, intermediate, and short axes of an ellipsoid that approximates the fragment. A uniform distribution of specimen sizes was sought, over the range 25 to 270 mm. The initial testing, begun with the iron-formation rock, was planned to provide an equal number of results for tests parallel to the long and the intermediate axis, to determine the effects caused by deviating from the originally suggested L-axis test orientation (ISRM, 1972). Experience showed that attempts to test parallel to L-axis were much more likely to be fruitless, with attendant loss of time, owing to events such as (i) progressive misalignment of the load points as one point slides down an inclined rock surface, opposite points on an axis usually not being on parallel surfaces, or (ii) splitting off a fragment from one side of a load point, which might occur several times without achieving a fracture through the specimen. Tests of metadiabase consequently were broadened to include tests parallel to S-axis, which turned out to offer the highest success rate. The chore of achieving L-axis tests led to their virtual abandonment in testing basalt specimens. No attempt was made to relate the load-axis orientation to the original in-place orientation of a specimen. Specimens were tested as found; no trimming was done.

To portray the fragment sizes and shapes, L vs. M and M vs. S are plotted in Fig. 6 for every fragment tested. The axis dimensions for the first 29 successful tests of iron-formation were determined before test by viewing a scale placed against the specimen and selecting a representative length (recorded to the nearest 2.5 mm). For these specimens, therefore, the initial distance D between the load points is an approximation taken equal to the appropriate axis dimension (L or M).

For the remaining 29 tests of iron-formation and all tests of metadiabase, dimensions (Fig. 7) were measured after test. A scale was held against the fracture surface to measure D, H, and F; the appropriate axis dimension was taken equal to D, since every test coincided with a selected axis. The final distance H between load points was ordinarily less than D, owing to penetration of the load points; mean H/D was 0.85, with standard

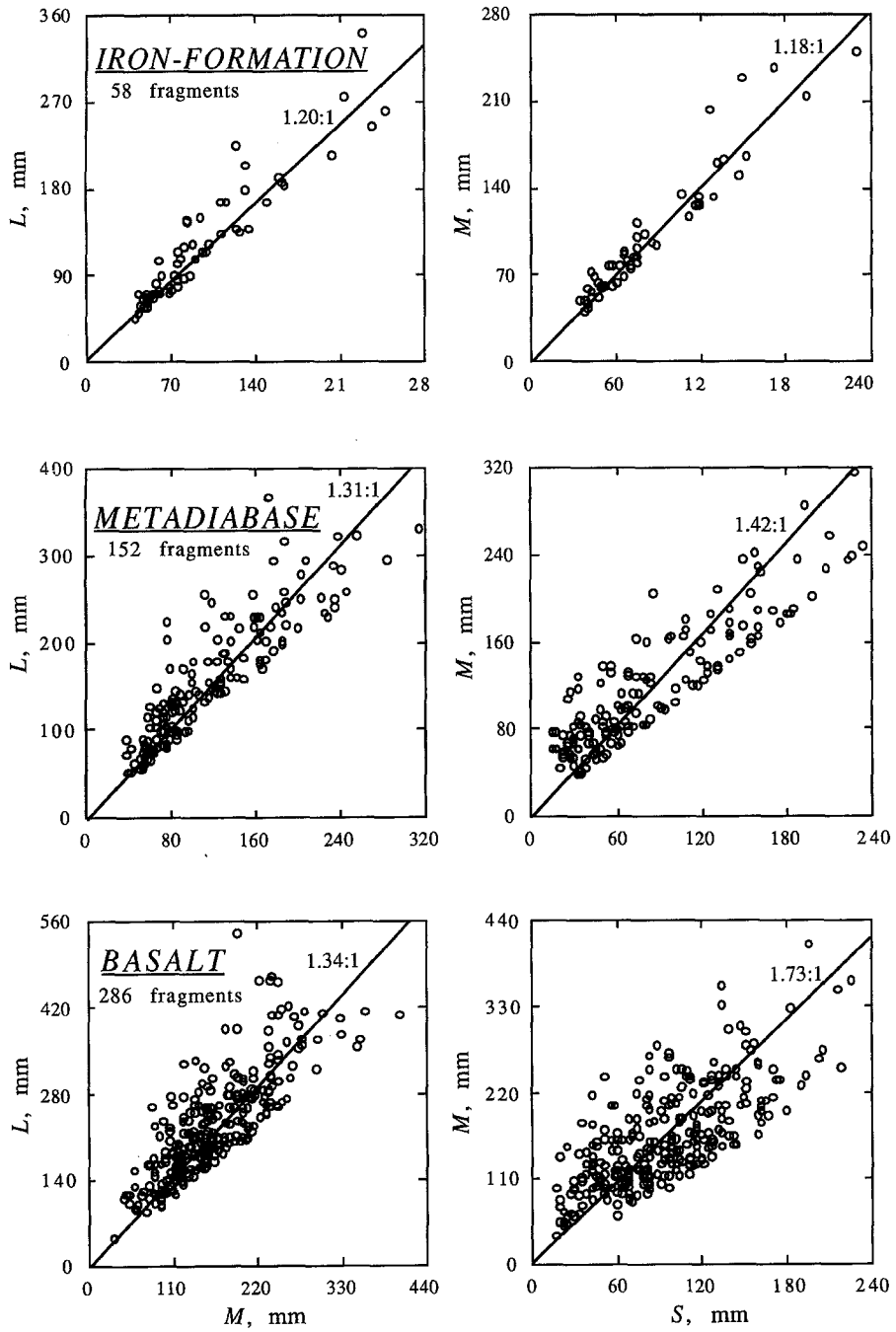

Fig. 6. PL tests, axis dimensions of the irregular-shape fragments. The line represents the median value of L/M or M/S

deviation 0.079, for 367 tests. On the fracture surface, the axis dimension of the approximating ellipse, measured perpendicular to the load axis, was recorded as F, no attempt being made to determine the deviation of the F-axis from the G-axis. To determine the two axis dimensions of the test specimen perpendicular to the load axis, the ruptured specimen was pieced together, a crude caliper was placed across the representative dimension, removed, and compared to a scale. For tests of basalt the (representative) axis dimensions were measured before test, and D, H, and F were measured after test. To avoid confusion, the best procedure is to assign the values of G and J in the office, based on the field-recorded load axis and values of L, M, and S.

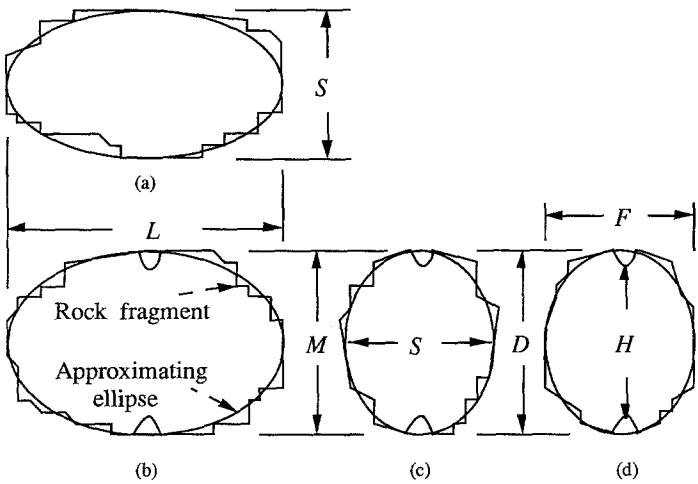

Fig. 7. Diametral cross sections of an irregular fragment, M-axis test, showing dimensions: **a** perpendicular to M-axis, **b** perpendicular to S-axis, **c** perpendicular to L-axis, **d** on the fracture surface. For M-axis load $D = M$, $G = S$, $J = L$, $F \geq S$. $D - H$ = penetration of load points during test

The fracture was characterized as (i) "direct", that is, passing through the load points, or "angle", the latter referring to the angle of deviation (measured to the nearest 5°) of the fracture surface from the load axis, and (ii) included notation of the estimated fraction of the fracture surface that appeared to follow a planar defect.

Rationale of Analysis of PL Tests

Following the same concepts employed in developing Eq. (1) for compression tests (Panek, 1981), one can expect to formulate PL strength as a similar product of a size effect by one or more shape effects, the independent variables being functions of the several dimensions. To obtain an explicit form of the equation for PL strength requires (i) identification of the most

important parameters and (ii) calculation of the values of K and the exponents c_i. The first of these tasks is facilitated by working with an expression of the following form:

$$P = K(M)^{c_M}(S)^{c_S}(D)^{c_D}, \tag{10}$$

where the factors on the right contain illustrative parameters, one or more of which are to be selected from L, M, S, D, H, F, G, J, U, W, X, Y, and V, all of which have dimension (length)^1. Ideally, the specimen dimensions D, G, and J simply comprise a redesignation of the axes to reflect specimen orientation with respect to load. That is, for L-axis loading $D = L$, $G = S$, and $J = M$; for M-axis loading $D = M$, $G = S$, and $J = L$; for S-axis loading $D = S$, $G = M$, and $J = L$. Owing to be described differences in measuring procedure, however, these equalities were not exact for all subsets of the data, and thus contributed to scatter in the results.

Although specimen volume was not directly determined in the experimental work, the geometric mean diameter of a specimen, $V = (LMS)^{1/3}$, provides a way to estimate the volume effect, since $LMS\,\pi/6$ is the volume of an ellipsoid having axes L, M, S. Similarly, (i) the minimum cross-sectional area of a point-load specimen through the load points can be approximated by $(U^2 = DG) \times \pi/4$, the area of an ellipse with axes D and G, (ii) the midsection (between load points) area of a specimen can be approximated by $(W^2 = GJ) \times \pi/4$, the area of an ellipse with axes G and J, and (iii) the area of the fracture surface can be approximated by $(X^2$ or $Y^2) \times \pi/4$, the area of an ellipse with axes D and F, or H and F, respectively.

Equation (10) can be converted later to an expression for stress (MPa) simply by dividing on both sides by the product of two of the dimensions that appear on the right side, or dividing by the square of one of them. For example, dividing through by SD and forming ratios, one can obtain the algebraically equivalent expression

$$P/SD = K(M/D)^{c_M}(S/D)^{c_S - 1}(1/D)^{2 - c_M - c_S - c_D}. \tag{10a}$$

Irrespective of the number of parameters included in the model, if the dependent variable is expressed in stress units (force/length^2) as function of dimensionless ratios formed from the independent variables, comparison of Eqs. (1), (10), and (10a) shows that the exponent of the factor 1/(representative dimension, w or D) is the size-effect exponent c_1 (retaining the notation of Eqs. (1), (2), and (6)), which thus takes the value

$$c_1 = 2 - (\text{Sum of exponents of individual dimensions in an equation for } P) \tag{11}$$

The value of c_1 calculated in this way is tabulated for all the analyses. To facilitate the numerical operations, the model to be analyzed, again using Eq. (10) as example, is linearized by the logarithmic transformation:

$$\log P = \log K + c_M \log M + c_S \log S + c_D \log D. \tag{12}$$

Least-squares solutions for log K and the coefficients of Eq. (12) were obtained by the standard statistical procedures of multilinear regression analysis. Solutions are given herein for models that contain a single fragment dimension parameter, two dimensions, and three dimensions, for specified rock type and specimen orientation with respect to load, seeking the best of these models.

PL Tests Analysis — Category Effects

In order to establish relationships and exponents that are valid for the several specimen loading orientations and rock types, as well as to determine the effects of the latter two factors, regression analyses were performed on data sets that include tests on more than one loading orientation and/or more than one rock type, inserting "dummy variables" (assigned the values 0 or 1) into Eq. (12) as appropriate (Draper and Smith, 1981), to represent the separate effects of the categorical parameters, orientation and rock type. To this end, the subscript L, M, or S denotes load applied parallel to the long, intermediate, or short specimen axis; and R, A, or B denotes a specimen of iron-formation, metadiabase, or basalt rock, respectively. M-axis tests and/or metadiabase tests are used as the common reference base. For example, the pooled data generated by M- and S-axis tests of basalt can be analyzed by Eq. (12) modified to evaluate also the effect of specimen orientation with respect to load:

$$\log P = \log K + Z_{SM}(ORIENT) + c_M \log M + c_S \log S + c_D \log D, \quad (12\,a)$$

where dummy variable $ORIENT = 0$ for an M-axis test, $ORIENT = 1$ for an S-axis test. The least-squares solution value of Z_{SM} reflects the difference in log K that is attributable to difference in specimen orientation when the effects of M, S, and D, reflected by the solution values of c_M, c_S, and c_D, are "averages" over the two orientations. Use of the dummy variable also minimizes the biases that would otherwise be present in the values of log K and the c_i due to the particular combinations of M, S, and D values that happened to be represented in the data set.

Dummy variables were employed to evaluate the following four Z effects (the coefficients of the dummy variables), the first two for orientation and the latter two for rock type:

$$\begin{aligned}
Z_{LM} &= (\log K_{LR} - \log K_{MR}) \text{ or } (\log K_{LA} - \log K_{MA}) \\
&\quad \text{or } (\log K_{LB} - \log K_{MB}) \\
Z_{SM} &= (\log K_{SR} - \log K_{MR}) \text{ or } (\log K_{SA} - \log K_{MA}) \\
&\quad \text{or } (\log K_{SB} - \log K_{MB}) \\
Z_{RA} &= (\log K_{LR} - \log K_{LA}) \text{ or } (\log K_{MR} - \log K_{MA}) \\
&\quad \text{or } (\log K_{SR} - \log K_{SA}) \\
Z_{BA} &= (\log K_{LB} - \log K_{LA}) \text{ or } (\log K_{MB} - \log K_{MA}) \\
&\quad \text{or } (\log K_{SB} - \log K_{SA}).
\end{aligned} \quad (13)$$

The three expressions for each Z are linked by "or" instead of "=" as reminder that, owing to scatter, the different expressions can be expected to yield different estimates for the same Z. From Eqs. (13), it follows that the K multipliers for Eq. (10), corresponding to the several combinations of specimen orientation and rock type, may be obtained from:

$$\begin{aligned}
\log K_{LA} &= \log K_{MA} + Z_{LM} \\
\log K_{SA} &= \log K_{MA} + Z_{SM} \\
\log K_{LR} &= \log K_{MA} + Z_{LM} + Z_{RA} \\
\log K_{MR} &= \log K_{MA} + Z_{RA} \\
\log K_{SR} &= \log K_{MA} + Z_{SM} + Z_{RA} \\
\log K_{LB} &= \log K_{MA} + Z_{LM} + Z_{BA} \\
\log K_{MB} &= \log K_{MA} + Z_{BA} \\
\log K_{SB} &= \log K_{MA} + Z_{SM} + Z_{BA}
\end{aligned} \tag{14}$$

The Z effects may be thought of as adjustments to $\log K$ that take into account differences as to specimen orientation and/or rock type, if they are present in the data, and thereby to obtain solution values for the dimension effects (the c's) that are valid for all the category effects (the Z's), that is, for any combination of orientation and rock type.

A closely related question is whether the dimension effects in the model are essentially the same for one loading direction or rock type as for another. For example, considering a one-dimension model, one may wish to determine whether a common slope $(\log P)/(\log S)$ is exhibited for L-axis tests and M-axis tests. This question is answered by reanalyzing the model with appropriate interaction terms inserted — the statistical test of "homogeneity of slopes". If one or more interactions are found to be statistically significant, the model is judged to be defective in representing the effects of the interacting variables.

Further Considerations in Analyzing the PL Test Data

Since the dependent regression variable is usually taken to be $\log P$ herein, the goodness of fit of any model to any subset of data can in general be compared to that of any other model either by the standard error of estimate (SE) or by the square of the multiple correlation ratio (R^2), both of which are tabulated herein. Apart from the uses of these indices for ranking models, SE is the value of one standard deviation above or below the values of $\log P$ estimated by the model, and hence SE is a direct measure of the scatter in the data; $R^2 \leq 1$ is the fraction of the total variation of $\log P$ that is attributable to the regression model. Values of R^2 are directly comparable only if they correspond to the same expression for the dependent regression variable. For example, changing the latter from $\log P$ to $\log (P/SD)$ changes the scale of the dependent variable and also changes the value of R^2. However, the value of SE is unaffected by this change, and hence SE is a more convenient measure of goodness of fit than is R^2, for comparing the models analyzed herein.

With regard to platen shape and fracture angle, preliminary analyses of the data indicated the following (these factors are quantitatively evaluated later):

1. For tests in which one or both loading platens was the flat-surface type, the maximum resistance of the specimens was, on average, slightly greater than if both platens were conical.
2. For tests in which the fracture surface deviated more than 7.5° from a line through the loading points, the maximum resistance was, on average, slightly less than for a fracture surface passing through the loading points.

Consequently, for the detailed analyses to find the best models, results of which are given in tables below, the test data were screened to include only the data for tests that conform to the specifications (i) both platens have the conical configuration, and (ii) the specimen fracture surface deviates less than 7.5° from a line through the loading points; these are the 357 "standard" tests in Table 3, which sets out the distribution of *PL* tests by category. In addition, 7 test results were excluded as "outliers"; these were anomalous low strengths, one *M*-axis test of metadiabase and six *S*-axis tests of basalt.

Table 3. Number of PL tests by category. Standard = two cone platens with fracture surface deviating $<7.5°$. *PF* = one flat platen, *FF* = both platens flat. Angle frac. = fracture surface that deviated 7.5°—17.5°

	Iron-formation	Metadiabase	Basalt	Total, std.
L-axis load	11 Standard	7 Standard	—	18
	4 PF	3 PF	1 PF	
	1 Angle frac.	4 Angle frac.	—	
M-axis load	34 Standard	44 Standard (excl. 1 outlier)	14 Standard	92
	—	1 PF	3 PF	
	2 Angle frac.	2 Angle frac.	1 Angle frac.	
S-axis load	—	80 Standard	167 Standard (excl. 6 outliers)	247
	—	1 PF	75 PF + 4 FF	
	—	2 Angle frac.	6 Angle frac.	
Total, std.	45	131	181	357

PL Tests — Results of Regression Analyses

A review of the regression results revealed no model that consistently exhibits the smallest *SE* among the one-dimension model forms or among the two-dimension forms. Goodness of fit to the data is not the only criterion, however. A desirable model characteristic is that it consistently tend to produce the same *c* values, irrespective of rock type or specimen orientation (apart from differences due to anisotropy). Consequently, for convenience in evaluating the consistency of the *c* values, regression solutions tabulated herein are grouped by model form, giving the values of the coefficients and the ranges of the *c* values found within each model form.

Table 4. Point load tests for single orientation and rock type, analyzed as function of a single dimension variable (*D, H, U, X,* or *V*). Models are designed by load axis (*L, M, S*) and rock type (*R, A, B*); suffix number indicates relative rank (*SE*) for goodness of fit. Under each regression coefficient is its standard error (parentheses). Iron-formation (*R*), metadiabase (*A*), basalt (*B*)

Model	log K^1	c_D	c_H	c_U	c_X	c_V	n	SE	R^2	c_1
LR 2	5.36 (1.62)	1.09 (0.34)	...	...	...	...	11	0.454	0.536	0.91 (0.34)
MR 4	5.54 (0.53)	1.15 (0.12)	...	...	...	...	34	0.366	0.743	0.85 (0.12)
MA 1	5.38 (0.42)	1.20 (0.09)	...	...	...	...	44	0.299	0.812	0.80 (0.09)
SA 1	6.51 (0.16)	1.06 (0.04)	...	...	...	...	80	0.222	0.902	0.94 (0.04)
MB 1	6.67 (1.05)	0.84 (0.22)	...	...	...	...	14	0.352	0.544	1.16 (0.22)
SB 3	6.36 (0.20)	1.02 (0.05)	...	...	...	...	167	0.334	0.735	0.98 (0.05)
	Range:	0.36								0.36
LR 1	5.76 (1.36)	...	1.04 (0.29)	...	...	...	11	0.431	0.583	0.96 (0.29)
MR 5	6.51 (0.48)	...	0.99 (0.12)	...	...	...	34	0.400[2]	0.693	1.01 (0.12)
MA 5	5.66 (0.43)	...	1.18 (0.10)	...	...	...	44	0.320	0.784	0.82 (0.10)
SA 2	6.72 (0.16)	...	1.05 (0.04)	...	...	...	80	0.240	0.886	0.95 (0.04)
MB 2	6.80 (1.03)	...	0.83 (0.22)	...	...	...	14	0.353	0.540	1.17 (0.22)
SB 5	6.72 (0.22)	...	0.98 (0.05)	...	...	...	167	0.367	0.680	1.02 (0.05)
		Range:	0.35							0.35
LR 5	6.05 (1.57)	...	...	0.98 (0.34)	...	...	11	0.482[2]	0.479	1.02 (0.34)
MR 1	5.39 (0.50)	...	...	1.20 (0.11)	...	...	34	0.342	0.776	0.80 (0.11)
MA 4	5.67 (0.41)	...	...	1.16 (0.09)	...	...	44	0.305	0.803	0.84 (0.09)
SA 3	5.27 (0.24)	...	...	1.26 (0.06)	...	...	80	0.260	0.866	0.74 (0.06)
MB 5	6.99 (1.00)	...	...	0.79 (0.22)	...	...	14	0.358	0.528	1.21 (0.22)
SB 1	4.97 (0.26)	...	...	1.24 (0.06)	...	...	167	0.330	0.742	0.76 (0.06)
			Range:	0.47						0.47
LR 3	5.59 (1.56)	...	...	...	1.06 (0.33)	...	11	0.457	0.532	0.94 (0.33)
MR 2	5.61 (0.48)	...	...	...	1.12 (0.11)	...	34	0.344	0.773	0.88 (0.11)
MA 2	5.36 (0.42)	...	...	...	1.20 (0.09)	...	44	0.301	0.809	0.80 (0.09)
SA 4	5.08 (0.27)	...	...	...	1.29 (0.06)	...	80	0.277[2]	0.848	0.71 (0.06)

Table 4. Continued

Model	log K[1]	c_D	c_H	c_U	c_X	c_V	n	SE	R^2	c_1
MB 3	6.83 (1.02)	...	...	...	0.81 (0.22)	...	14	0.354	0.538	1.19 (0.22)
SB 2	4.74 (0.28)	...	...	...	1.28 (0.06)	...	167	0.331	0.740	0.72 (0.06)
				Range:	0.48					0.48
LR 4	5.84 (1.57)	...	...	...	...	1.02 (0.34)	11	0.470	0.504	0.98 (0.34)
MR 3	5.27 (0.51)	...	...	...	...	1.20 (0.12)	34	0.345	0.772	0.80 (0.12)
MA 3	5.44 (0.42)	...	...	...	...	1.17 (0.09)	44	0.305	0.804	0.83 (0.09)
SA 5	4.56 (0.32)	...	...	...	...	1.36 (0.07)	80	0.294[2]	0.829	0.64 (0.07)
MB 4	6.31 (1.16)	...	...	...	...	0.90 (0.24)	14	0.354	0.537	1.10 (0.24)
SB 4	4.38 (0.31)	...	...	...	...	1.29 (0.06)	167	0.344	0.719	0.71 (0.06)
					Range:	0.46				0.46

[1] Subscript of K is the same as the two-letter model designation.
[2] Mediocre fit to the date: SE exceeds by >0.05 the best solution for the same subset.

The results for the six main category groups (separate specimen orientation and rock type) are given in Table 4 for the five best one-dimension model forms. Each model has the general form of Eq. (12) with only one dimension variable. The 7 L-axis tests of metadiabase are not analyzed as a separate group, owing to the small number of tests. Models are denoted by L, M, or S (load axis), R, A, or B (iron-formation, metadiabase, or basalt); and a number from 1 to 5 indicating the SE rank of the model within its data subset (combination of orientation and rock type), among the parameters D, H, U, X, and V. For example, MB1 has smaller SE than any other model of M-axis tests of basalt listed in Table 4. Of the five model forms in Table 4, considering the criteria of consistency and goodness of fit, the function of D is rated the best single-dimension form.

Substantial differences exist as to SE among rock types and among orientations, which should be borne in mind in comparing SE values other than within the same rock type and orientation. Comparison of the scatters within test category groups can be based on the smallest SE value within each of the six main categories: Model SA1 shows the smallest SE (0.222), followed in order by models MA1, SB1, MR1, MB1, and LR1. A statistical test indicates that the within-group scatters are nonhomogeneous, L-axis tests of iron-formation showing SE above the average for the six groups and S-axis tests of metadiabase below-average SE.

For tests of iron-formation and metadiabase the axis dimension parallel to the load was recorded as (taken equal to) the dimension D on the broken specimens, and hence for these two rock types the c_D values are taken

Table 5. Point load tests pooled by rock type (*R, A, B*), by orientation (*L, M, S*), and all pooled (*P*), analyzed as function of a single dimension variable (*D, H, U, X,* or *Y*). Iron-formation (*R*); metadiabase (*A*), basalt (*B*)

Model	log K[1]	Z_{LM}	Z_{SM}	Z_{RA}	Z_{BA}	c_D	c_H	c_U	c_X	c_Y	n	SE	R^2	c_1
R 4	5.58 (0.51)	−0.44 (0.14)	...	...	...	1.14 (0.11)	...	...	...	...	45	0.383	0.703	0.86 (0.11)
A 1	5.89 (0.18)	−0.41 (0.10)	0.48 (0.06)	...	...	1.09 (0.04)	...	...	...	...	131	0.256	0.871	0.91 (0.04)
B 1	5.84 (0.24)	...	0.56 (0.10)	...	...	1.01 (0.05)	...	...	...	...	181	0.335	0.725	0.99 (0.05)
L 4	5.64 (1.04)	...	...	−0.12 (0.19)	...	1.06 (0.21)	...	...	...	...	18	0.402	0.626	0.94 (0.21)
M 3	5.66 (0.33)	...	...	−0.09 (0.08)	−0.42 (0.10)	1.14 (0.07)	...	...	...	...	92	0.334	0.772	0.86 (0.07)
S 1	6.59 (0.14)	...	...	...	−0.28 (0.04)	1.04 (0.03)	...	...	...	...	247	0.302	0.796	0.96 (0.03)
P 1	6.00 (0.15)	−0.40 (0.08)	0.50 (0.05)	−0.09 (0.06)	−0.31 (0.04)	1.06 (0.03)	...	...	...	...	357	0.315	0.781	0.94 (0.03)
					Range:	0.13								0.13
R 5	6.48 (0.45)	−0.51 (0.15)	...	...	...	...	1.00 (0.11)	...	...	...	45	0.402	0.671	1.00 (0.11)
A 2	6.11 (0.19)	−0.51 (0.11)	0.49 (0.06)	...	...	...	1.08 (0.04)	...	...	...	131	0.273	0.853	0.92 (0.04)
B 5	6.14 (0.25)	...	0.61 (0.11)	...	...	...	0.97 (0.05)	...	...	...	181	0.366	0.673	1.03 (0.05)
L 3	5.80 (0.94)	...	...	−0.01 (0.19)	...	...	1.04 (0.20)	...	...	...	18	0.386	0.657	0.96 (0.20)
M 5	6.21 (0.32)	...	...	0.02 (0.09)	−0.48 (0.11)	...	1.06 (0.07)	...	...	...	92	0.358	0.738	0.94 (0.07)
S 5	6.88 (0.14)	...	...	...	−0.28 (0.05)	...	1.00 (0.04)	...	...	...	247	0.332	0.754	1.00 (0.04)
P 5	6.34 (0.15)	−0.49 (0.09)	0.50 (0.06)	0.04 (0.07)	−0.32 (0.04)	...	1.02[2] (0.03)	...	...	...	357	0.341	0.744	0.98 (0.03)
						Range:	0.11							0.11
R 3	5.56 (0.49)	−0.37 (0.13)	...	...	...	...	...	1.16 (0.11)	...	...	45	0.375	0.714	0.84 (0.11)
A 3	5.41 (0.22)	−0.34 (0.11)	0.08 (0.05)	...	...	...	...	1.21 (0.05)	...	...	131	0.277	0.849	0.79 (0.05)
B 2	5.05 (0.27)	...	0.08 (0.09)	...	...	...	...	1.21[3] (0.06)	...	...	181	0.335	0.725	0.79 (0.06)
L 5	6.08 (0.97)	...	...	−0.11 (0.20)	...	...	...	1.00 (0.21)	...	...	18	0.408	0.615	1.00 (0.21)
M 2	5.79 (0.32)	...	...	−0.08 (0.08)	−0.39 (0.10)	...	...	1.13[4] (0.07)	...	...	92	0.330	0.777	0.87 (0.07)
S 2	5.33 (0.18)	...	...	...	−0.40 (0.04)	...	...	1.25 (0.04)	...	...	247	0.308	0.787	0.75 (0.04)
P 2	5.45 (0.16)	−0.36 (0.08)	0.08 (0.05)	−0.07 (0.06)	−0.39 (0.04)	...	...	1.20[5] (0.04)	...	...	357	0.319	0.776	0.80 (0.04)
							Range:	0.25						0.25

Table 5. Continued

Model	log K[1]	Z_{LM}	Z_{SM}	Z_{RA}	Z_{BA}	c_D	c_H	c_U	c_X	c_Y	n	SE	R^2	c_1
R 1	5.65 (0.47)	−0.29 (0.13)	...	...	...	...	...	...	1.11 (0.10)	...	45	0.367	0.726	0.89 (0.10)
A 4	5.14 (0.23)	−0.26 (0.12)	0.14 (0.06)	...	...	...	...	...	1.24 (0.05)	...	131	0.283	0.842	0.76 (0.05)
B 3	4.82 (0.28)	...	0.09 (0.09)	...	...	...	...	...	1.24[3] (0.06)	...	181	0.336	0.723	0.76 (0.06)
L 2	5.79 (0.91)	...	...	−0.15 (0.18)	...	...	...	...	1.05 (0.19)	...	18	0.376	0.673	0.95 (0.19)
M 1	5.71 (0.32)	...	...	−0.11 (0.08)	−0.34 (0.10)	...	...	...	1.12[4] (0.07)	...	92	0.327	0.781	0.88 (0.07)
S 3	5.12 (0.19)	...	...	...	−0.40 (0.05)	...	...	...	1.28 (0.04)	...	247	0.314	0.779	0.72 (0.04)
P 3	5.26 (0.17)	−0.30 (0.08)	0.12 (0.05)	−0.10 (0.06)	−0.37 (0.04)	...	...	...	1.22[5] (0.04)	...	357	0.321	0.773	0.78 (0.04)
								Range:	0.23					0.23
R 2	6.06 (0.44)	−0.34 (0.13)	...	...	...	...	...	...	...	1.05 (0.10)	45	0.373	0.718	0.95 (0.10)
A 5	5.23 (0.24)	−0.31 (0.12)	0.15 (0.06)	...	...	...	...	...	...	1.24 (0.05)	131	0.288	0.837	0.76 (0.05)
B 4	4.90 (0.29)	...	0.13 (0.10)	...	...	...	...	...	...	1.24[3] (0.06)	181	0.346	0.707	0.76 (0.06)
L 1	5.88 (0.86)	...	...	−0.10 (0.18)	...	...	...	...	...	1.04[4] (0.18)	18	0.368	0.686	0.96 (0.18)
M 4	5.94 (0.31)	...	...	−0.05 (0.08)	−0.37 (0.10)	...	...	...	...	1.09 (0.07)	92	0.336	0.770	0.91 (0.07)
S 4	5.23 (0.19)	...	...	...	−0.41 (0.05)	...	...	...	...	1.28 (0.05)	247	0.323	0.767	0.72 (0.05)
P 4	5.41 (0.17)	−0.35 (0.09)	0.13 0.05	−0.03 0.07	−0.38 (0.04)	...	...	...	...	1.21[5] (0.04)	357	0.329	0.761	0.79 (0.04)
									Range:	0.24				0.24

[1] Subscript of K is *MR, MA, MB, LA, MA, SA* or *MA*, respectively, for model *R, A, B, L, M, S,* or *P.*
[2] This variable exhibits interaction ($\alpha < 0.05$) with Z_{BA}.
[3] This variable exhibits interaction ($\alpha < 0.05$) with Z_{SM}.
[4] This variable exhibits interaction ($0.05 < \alpha < 0.10$) with Z_{BA}.
[5] This variable exhibits interaction ($0.05 < \alpha < 0.10$) with Z_{SM}.

equal to the c_L values for L-axis tests, equal to the c_M values for M-axis tests, and equal to the c_S values for S-axis tests.

The six main combinations of specimen orientation and rock type were analyzed using models containing two dimension parameters, but the solutions are not tabulated herein because these models generally failed to demonstrate statistically significant improvement in fit to the data as compared with the appropriate single-dimension models of Table 4 — very few models showed $c_i/(\text{std dev } c_i) > 2$ for both variables. Consequently, we consider next the analyses of pooled data.

For each of the five best one-dimension model forms, a solution is listed in Table 5 (i) for each rock type, pooling the test results for all orien-

Table 6. Point load tests pooled by rock type (*R, A, B*), orientation (*L, M, S*), and all pooled (*P*). Best functions of two dimension variables

Model	log K^1	Z_{LM}	Z_{SM}	Z_{RA}	Z_{BA}	c_L	c_D	c_H	c_G	c_F	c_W	n	SE	R^2	c_1
R 1	5.63	−0.30	...	...	...	...	0.60	...	...	0.52	...	45	0.372	0.727	0.88
	(0.49)	(0.15)					(0.31)			(0.27)					(0.11)
A 1	5.58	−0.37	0.39	...	...	...	0.97[2]	...	...	0.19	...	131	0.251	0.876	0.85
	(0.22)	(0.10)	(0.07)				(0.06)			(0.08)					(0.05)
B 2	5.15	...	0.34	...	...	...	0.85	...	...	0.31	...	181	0.321	0.750	0.84
	(0.28)		(0.11)				(0.06)			(0.08)					(0.06)
L 2	5.88	...	...	−0.16	...	...	0.41	...	...	0.62	...	18	0.389	0.674	0.96
	(1.01)			(0.19)			(0.49)			(0.43)					(0.21)
M 1	5.63	...	...	−0.10	−0.37	...	0.79	...	...	0.35	...	92	0.325	0.787	0.86
	(0.32)			(0.08)	(0.10)		(0.16)			(0.15)					(0.07)
S 2	5.85	...	...	...	−0.34	...	0.90[3]	...	...	0.27[4]	...	247	0.292	0.811	0.83
	(0.21)				(0.04)		(0.05)			(0.06)					(0.04)
P 1	5.53	−0.36	0.34	−0.09	−0.34	...	0.88	...	...	0.28	...	357	0.303	0.798	0.84
	(0.17)	(0.08)	(0.06)	−(0.06)	(0.04)		(0.04)			(0.05)					(0.03)
						Range:	0.56			0.44					0.13
R 5	5.44	−0.35	...	...	...	0.36	0.79	...	...	...	...	45	0.385	0.707	0.85
	(0.54)	(0.18)				(0.46)	(0.46)								(0.12)
A 3	5.59	−0.37	0.41	...	...	0.15	0.99	...	...	...	...	131	0.254	0.874	0.86
	(0.24)	(0.11)	(0.07)			(0.08)	(0.07)								(0.05)
B 3	4.87	...	0.41	...	...	0.36	0.83	...	...	...	...	181	0.321	0.749	0.81
	(0.33)		(0.10)			(0.09)	(0.06)								(0.06)
L 3	5.64	...	...	−0.12	...	0.53	0.53	...	...	...	...	18	0.402	0.626	0.94
	(1.04)			(0.19)		(0.11)	(0.11)								(0.21)
M 4	5.50	...	...	−0.07	−0.45	0.27	0.88	...	...	...	...	92	0.332	0.778	0.84
	(0.34)			(0.08)	(0.11)	(0.19)	(0.19)								(0.07)
S 3	5.74	...	...	...	−0.35	0.29[3]	0.89[3]	...	...	...	...	247	0.292	0.810	0.82
	(0.24)				(0.04)	(0.07)	(0.05)								(0.05)
P 4	5.44	−0.35	0.37	−0.06	−0.36	0.28	0.89	...	...	...	...	357	0.307	0.793	0.83
	(0.19)	(0.08)	(0.06)	(0.06)	(0.04)	(0.06)	(0.05)								(0.04)
						Range:	0.38	0.46							0.13
R 3	5.57	−0.36	...	...	...	...	0.56[2]	...	0.60[2]	...	...	45	0.380	0.714	0.84
	(0.50)	(0.15)					(0.46)		(0.47)						(0.11)
A 4	5.71	−0.39	0.39	...	...	...	0.98	...	0.16	...	...	131	0.254	0.874	0.87
	(0.21)	(0.10)	(0.08)				(0.08)		(0.09)						(0.05)
B 4	5.29	...	0.33	...	...	...	0.83	...	0.31	...	...	181	0.322	0.747	0.86
	(0.27)		(0.11)				(0.06)		(0.08)						(0.06)
L 5	5.71	...	...	−0.11	...	...	0.95	...	0.10	...	...	18	0.416	0.627	0.95
	(1.13)			(0.20)			(0.67)		(0.59)						(0.22)
M 3	5.72	...	...	−0.08	−0.40	...	0.75[5]	...	0.39[5]	...	...	92	0.331	0.779	0.86
	(0.33)			(0.08)	(0.10)		(0.25)		(0.24)						(0.07)
S 4	5.92	...	...	...	−0.34	...	0.87	...	0.28[3]	...	...	247	0.292	0.810	0.84
	(0.20)				(0.04)		(0.05)		(0.07)						(0.04)
P 3	5.65	−0.39	0.32	−0.07	−0.35	...	0.87	...	0.28	...	...	357	0.306	0.794	0.85
	(0.16)	(0.08)	(0.06)	(0.06)	(0.04)		(0.05)		(0.06)						(0.03)
						Range:	0.42		0.50						0.11

Table 6. Continued

Model	log K[1]	Z_{LM}	Z_{SM}	Z_{RA}	Z_{BA}	c_L	c_D	c_H	c_G	c_F	c_W	n	SE	R^2	c_1
R 3	5.40 (0.51)	−0.21 (0.21)	...	...	...	...	0.27 (0.60)	...	...	...	0.90 (0.60)	45	0.377	0.718	0.83 (0.11)
A 2	5.59 (0.23)	−0.36 (0.11)	0.38 (0.07)	...	...	...	0.96 (0.08)	...	...	...	0.19 (0.09)	131	0.253	0.875	0.85 (0.05)
B 1	4.94 (0.31)	...	0.33 (0.11)	...	...	...	0.79 (0.07)	...	...	...	0.40 (0.09)	181	0.319	0.753	0.81 (0.06)
L 4	5.78 (1.09)	...	...	−0.12 (0.20)	...	...	0.66 (0.79)	...	...	...	0.38 (0.74)	18	0.412	0.633	0.95 (0.22)
M 2	5.54 (0.33)	...	...	−0.07 (0.08)	−0.44 (0.10)	...	0.56 (0.29)	...	...	...	0.60 (0.29)	92	0.328	0.783	0.84 (0.07)
S 1	5.68 (0.23)	...	...	...	−0.36 (0.04)	...	0.85[3] (0.05)	...	...	...	0.34[3] (0.07)	247	0.290	0.813	0.81 (0.05)
P 2	5.44 (0.18)	−0.34 (0.08)	0.31 (0.06)	−0.06 (0.06)	−0.37 (0.04)	...	0.84 (0.05)	...	...	...	0.34 (0.06)	357	0.304	0.797	0.82 (0.04)
						Range:	0.69				0.71				0.14
R 2	6.02 (0.45)	−0.29 (0.16)	...	...	...	...	...	0.40 (0.25)	...	0.65 (0.24)	...	45	0.376	0.720	0.95 (0.10)
A 5	5.65 (0.23)	−0.44 (0.11)	0.37 (0.07)	...	...	...	...	0.92 (0.06)	...	0.25 (0.08)	...	131	0.264	0.864	0.83 (0.05)
B 5	5.14 (0.30)	...	0.30 (0.11)	...	...	...	...	0.76 (0.06)	...	0.42 (0.08)	...	181	0.340	0.719	0.82 (0.06)
L 1	5.87 (0.93)	...	...	−0.09 (0.20)	...	...	...	0.54 (0.48)	...	0.50 (0.44)	...	18	0.381	0.686	0.96 (0.19)
M 5	5.95 (0.31)	...	...	−0.04 (0.08)	−0.38 (0.11)	...	...	0.60 (0.15)	...	0.49 (0.14)	...	92	0.337	0.770	0.91 (0.07)
S 5	5.80 (0.23)	...	...	...	−0.36 (0.05)	...	...	0.82[4] (0.05)	...	0.37[4] (0.06)	...	247	0.311	0.785	0.80 (0.05)
P 5	5.64 (0.17)	−0.42 (0.09)	0.29 (0.06)	0.01 (0.06)	−0.37 (0.04)	...	...	0.80 (0.04)	...	0.37 (0.05)	...	357	0.320	0.775	0.84 (0.04)
							Range:	0.52		0.40					0.16

[1] Subscript of K is *MR, MA, MB, LA, MA, SA* or *MA*, respectively, for model *R, A, B, L, M, S,* or *P.*
[2] This variable exhibits interaction ($0.05 < \alpha < 0.10$)) with Z_{LM}.
[3] This variable exhibits interaction ($0.05 < \alpha < 0.10$) with Z_{BA}.
[4] This variable exhibits interaction ($\alpha < 0.05$) with Z_{BA}.
[5] This variable exhibits interaction ($0.05 < \alpha < 0.10$) with Z_{RA}.

tations (including the small set of 7 *L*-axis tests of metadiabase), (ii) for each test orientation, pooling the test results for all rock types, and (iii) for the pooling of all orientations and rock types. Where two or three test orientations (or rock types) are included in the data group, one or two dummy variables, respectively, were included in the model so that the solution value of c is appropriate to all the orientations; such a solution yields also an estimate of the orientation effect Z_{LM} and/or Z_{SM} (or of Z_{RA} and/or Z_{BA}). Similarly, where all the test data are pooled, four dummy variables were used so that c is appropriate to all three orientations and all three rock types; and the solution yields estimates of two orientation effects and two rock type effects.

Table 7. Point load tests pooled by rock type (*R, A, B*), orientation (*L, M, S*), and all pooled (*P*). Best functions of two dimension variables

Model	log K^1	Z_{LM}	Z_{SM}	Z_{RA}	Z_{BA}	c_L	c_D	c_H	c_G	c_F	c_J	n	SE	R^2	c_1
R 1	5.58	−0.28	...	...	...	0.13	0.50	...	...	0.49	...	45	0.376	0.727	0.88
	(0.53)	(0.18)				(0.47)	(0.48)			(0.29)					(0.11)
A 1	5.53	−0.36	0.39	...	...	0.05[2]	0.96[2]	...	...	0.16	...	131	0.252	0.877	0.84
	(0.24)	(0.10)	(0.07)			(0.10)	(0.07)			(0.10)					(0.05)
B 1	4.82	...	0.33	...	...	0.22	0.80	...	...	0.20	...	181	0.318	0.755	0.79
	(0.33)		(0.11)			(0.11)	(0.07)			(0.10)					(0.06)
L 1	5.88	...	...	−0.16	...	0.21	0.21	...	...	0.62	...	18	0.389	0.674	0.96
	(1.01)			(0.19)		(0.25)	(0.25)			(0.43)					(0.21)
M 1	5.52	...	...	−0.09	−0.40	0.19	0.64	...	...	0.32	...	92	0.325	0.789	0.85
	(0.34)			(0.08)	(0.11)	(0.19)	(0.22)			(0.15)					(0.07)
S 1	5.62	...	...	...	−0.36	0.17	0.86[3]	...	...	0.17	...	247	0.290	0.813	0.80
	(0.24)				(0.04)	(0.09)	(0.05)			(0.08)					(0.05)
P 1	5.39	−0.35	0.32	−0.08	−0.36	0.12	0.85	...	...	0.22	...	357	0.302	0.799	0.81
	(0.19)	(0.08)	(0.06)	(0.06)	(0.04)	(0.08)	(0.05)			(0.07)					(0.04)
					Range:	0.17	0.75			0.46					0.17
R 4	5.45	−0.28	...	...	...	0.32[4]	0.27[4]	...	0.58[4]	...	...	45	0.382	0.718	0.83
	(0.53)	(0.19)				(0.45)	(0.62)		(0.47)						(0.12)
A 3	5.59	−0.37	0.39	...	...	0.11	0.96	...	0.08	...	...	131	0.254	0.875	0.85
	(0.24)	(0.11)	(0.08)			(0.11)	(0.08)		(0.12)						(0.05)
B 2	4.91	...	0.33	...	...	0.23	0.79	...	0.17	...	...	181	0.320	0.753	0.80
	(0.33)		(0.11)			(0.12)	(0.07)		(0.10)						(0.06)
L 4	5.71	...	...	−0.11	...	0.47	0.47	...	0.10	...	...	18	0.416	0.627	0.95
	(1.13)			(0.20)		(0.34)	(0.34)		(0.59)						(0.22)
M 2	5.57	...	...	−0.07	−0.43	0.26	0.53[5]	...	0.37[5]	...	...	92	0.329	0.783	0.85
	(0.34)			(0.08)	(0.11)	(0.19)	(0.30)		(0.24)						(0.07)
S 1	5.68	...	...	...	−0.36	0.17	0.85[3]	...	0.17	...	...	247	0.290	0.813	0.81
	(0.24)				(0.04)	(0.09)	(0.05)		(0.09)						(0.05)
P 3	5.45	−0.36	0.31	−0.06	−0.37	0.16	0.84	...	0.18	...	...	357	0.305	0.797	0.82
	(0.19)	(0.08)	(0.06)	(0.06)	(0.04)	(0.08)	(0.05)		(0.08)						(0.04)
					Range:	0.36	0.69		0.50						0.16
R 3	5.44	−0.24	...	...	...	...	0.26	...	0.57[4]	...	0.34	45	0.382	0.719	0.83
	(0.33)	(0.22)					(0.60)		(0.47)		(0.44)				(0.12)
A 2	5.57	−0.35	0.39	...	...	...	0.96	...	0.06	...	0.13	131	0.254	0.875	0.85
	(0.24)	(0.11)	(0.08)				(0.08)		(0.12)		(0.11)				(0.05)
B 2	4.91	...	0.33	...	...	...	0.79	...	0.17	...	0.23	181	0.320	0.753	0.80
	(0.33)		(0.11)				(0.07)		(0.10)		(0.12)				(0.06)
L 3	5.36	...	...	−0.18	...	...	0.32	...	−0.60	...	1.41	18	0.411	0.662	0.87
	(1.16)			(0.21)			(0.85)		(0.85)		(1.22)				(0.23)
M 2	5.57	...	...	−0.07	−0.43	...	0.53[5]	...	0.37[5]	...	0.26	92	0.329	0.783	0.85
	(0.34)			(0.08)	(0.11)		(0.30)		(0.24)		(0.19)				(0.07)
S 1	5.68	...	...	...	−0.36	...	0.85[3]	...	0.17	...	0.17	247	0.290	0.813	0.81
	(0.24)				(0.04)		(0.05)		(0.09)		(0.09)				(0.05)
P 2	5.44	−0.34	0.31	−0.06	−0.37	...	0.84[3]	...	0.17[2]	...	0.17	357	0.304	0.797	0.82
	(0.19)	(0.08)	(0.06)	(0.06)	(0.04)		(0.05)		(0.08)		(0.08)				(0.04)
						Range:	0.70		1.17		1.28				0.07

Table 7. Continued

Model	log K[1]	Z_{LM}	Z_{SM}	Z_{RA}	Z_{BA}	c_L	c_D	c_H	c_G	c_F	c_J	n	SE	R^2	c_1
R 2	5.74	−0.24	...	...	...	−0.31	...	0.25	...	0.53	...	45	0.378	0.724	0.91
	(0.57)	(0.18)				(0.38)		(0.32)		(0.28)					(0.11)
A 4	5.57	−0.42	0.35	...	...	0.09	...	0.90	...	0.20	...	131	0.264	0.865	0.82
	(0.26)	(0.11)	(0.07)			(0.11)		(0.07)		(0.10)					(0.05)
B 4	4.70	...	0.29	...	...	0.29	...	0.70	...	0.26	...	181	0.335	0.729	0.75
	(0.34)		(0.11)			(0.11)		(0.06)		(0.10)					(0.07)
L 2	5.92	...	...	−0.09	...	−0.11	...	0.62	...	0.52	...	18	0.396	0.687	0.97
	(1.03)			(0.22)		(0.88)		(0.87)		(0.47)					(0.21)
M 4	5.66	...	...	−0.05	−0.43	0.34	...	0.39	...	0.40	...	92	0.332	0.779	0.87
	(0.35)			(0.08)	(0.11)	(0.18)		(0.18)		(0.15)					(0.07)
S 4	5.50	...	...	...	−0.39	0.22	...	0.78[6]	...	0.24	...	247	0.308	0.790	0.76
	(0.26)				(0.05)	(0.09)		(0.05)		(0.08)					(0.05)
P 4	5.43	−0.40	0.27	0.02	−0.39	0.18	...	0.75[3]	...	0.26	...	357	0.318	0.778	0.80
	(0.20)	(0.09)	(0.06)	(0.06)	(0.04)	(0.08)		(0.05)		(0.07)					(0.04)
					Range:	0.45		0.65		0.33					0.22

[1] Subscript of K is *MR, MA, MB, LA, MA, SA* or *MA*, respectively, for model *R, A, B, L, M, S,* or *P.*
[2] This variable exhibits interaction ($0.05 < \alpha < 0.10$) with Z_{LM}.
[3] This variable exhibits interaction ($0.05 < \alpha < 0.10$) with Z_{BA}.
[4] This variable exhibits interaction ($\alpha < 0.05$) with Z_{LM}.
[5] This variable exhibits interaction ($0.05 < \alpha < 0.10$) with Z_{RA}.
[6] This variable exhibits interaction ($\alpha < 0.05$) with Z_{BA}.

To clarify the scheme used in tabulating the model solutions, consider model P1 of Table 5, a representation of the all-pooled tests. The listed solution values for P1 express all 9 category combinations of specimen orientation and rock type in accordance with Eqs. (12) and (14), two examples being

$$\log P = 6.00 + 1.06 \log D, \tag{15a}$$

for M-axis tests of metadiabase, and

$$\log P = 6.00 + 0.50 - 0.31 + 1.06 \log D, \tag{16a}$$

for S-axis tests of basalt, which are respectively the logarithmic forms of

$$P = 403\ D^{1.06}, \tag{15b}$$

and

$$P = 488\ D^{1.06}, \tag{16b}$$

where P is in Newtons, D in millimeters. These equations estimate log P with standard error 0.315, and c_D with standard error 0.03. The exponent of D implies that the corresponding size-effect exponent $c_1 = 2 - 1.06 = 0.94$. For a sample size greater than 30, the statistical "t" distribution implies a 95% confidence interval about an estimated parameter approximately equal to plus or minus twice its standard error; an additional interpretation is that the estimated parameter may be considered not significantly different from zero if it is less than about twice its standard error.

Where analysis was made of pooled data, using a model that included the appropriate category variable(s), orientation and/or rock type, evaluation was made also of the probability of statistical interaction between the dimension variable(s) and the category variable(s) in the model (a statistical test for homogeneity of slopes). At the foot of Table 5 are given values of α for those instances in which the probability is less than 0.10 that the calculated interaction effect exhibited in the data is simply due to random variation. For example, $\alpha < 0.05$ for interaction with Z_{BA} suggests strong probability of the interaction, indicating that the effect (on specimen resistance) of rock type is not consistently the same for the basalt (B) tests as for the metadiabase (A) tests; $0.05 < \alpha < 0.10$ is herein interpreted to imply that better consistency would be desirable. Thus, in the presence of interaction the c values can be expected to vary with the corresponding category variable. Models that do not exhibit such interactions can be expected to show more-stable c values. The statistical interaction test complements the evaluation of c-value range — the former evaluates the statistical probability of the existence of an interaction effect, and the latter considers the total variability of the c values due to all sources, including interaction.

In Table 5, considering the three criteria of low SE, small range of c values, and absence of interaction effects, the model form function of D is again (as in Table 4) rated the best single-dimension form.

Tables 6 and 7 list the solutions for the best functions of two and of three dimension variables, respectively, for test data analyzed by rock type (pooled orentations), by test orientation (pooled rock types), and for all data pooled. Several of the models (indicated by footnote) exhibit statistical interaction between one or both dimensions and one or more specimen orientations and/or rock types, indicating some degree of inadequacy in achieving a consistent fit to the data.

In Table 7 little weight can be given to the c-value consistency of the three dimension variables, as most are not statistically significant. The function of (L, D, F) ranks highest for goodness of fit to the data, and it is one of the two model forms that is free of the very undesirable interactions for all-data-pooled, and hence it is rated the best three-dimension form. The model form function of (L, D, G) is rated better than (L, H, F) because of its better fit to the data, and, for the all-data-pooled, better c_1 consistency and the absence of interaction. The model form function of (D, G, J), the fully explicit form of the function of (D, W), Table 6, exhibits almost the same numerical values as the function of (L, D, G) and by far the best c_1 consistency.

Versions of Tables 4 to 7 were also prepared, but not reproduced herein, for regression solutions in which for the basalt test data the initial distance D is taken equal to the appropriate axis dimensions measured before test, as is necessary for the first 29 tests of iron-formation. Only the basalt models containing D are affected thereby. Interestingly, SE is decreased in most instances, by about 0.003. Coefficients (Z's and c's) are changed about 0.02 on average, not enough to be statistically significant.

6. Discussion of Point Load Test Results

Even though they are actually functions of more than one variable, the special dimension variables U, W, X, Y, and V are for simplicity expressed in the form of (length)^1 and their model solutions tabulated with the group of one-variable models; thus the values of c_1 can be calculated by the simple expression of Eq. (11). It is easily shown that replacing the variable D, for example, by a variable $A = D^m$ alters the solution values given for any function-of-D model in Tables 4 and 5 only in that $c_A = c_D/m$ and (standard error of c_A) = (standard error of c_D)$/m$, none of the other solution values being affected by the substitution. Consequently, since a one-dimension-variable model function of D is found to be superior to a one-dimension-variable model that is a function of U, W, X, Y, or V (Tables 4 and 5), it follows that a one-dimension-variable model based on the *square* of D, for example, is superior to any one-dimension-variable model based on U^2, W^2, X^2, Y^2, or V^2, and therefore that expressing PL strength as function of D^2 is superior to expressing it as function of any of the following: Minimum cross-sectional area through the load points, midsection cross-sectional area, fracture surface area, or specimen volume. On the other hand, any two-dimension-variable model in Table 6, where the two c's are free to take unlike values, has much smaller SE than a model based on the square of either one of those two, Table 5.

In general, as the number of dimension variables is increased in the model, the indicated size-effect exponent decreases, as does the SE. This can be illustrated by comparing the best-fitting models of the all-pooled data, P1 of Table 5, P1 of Table 6, and P1 of Table 7. Dividing through by D^2 in each of these to express the PL strength in stress units as was done to obtain Eq. (10a), these models may be presented respectively as follows:

$$P/D^2 = K(1/D)^{0.939} \qquad (SE = 0.315) \qquad (17)$$
$$\qquad\qquad (0.030) \quad \text{(standard error of exponent)}$$

$$P/D^2 = K(1/D)^{0.837}(F/D)^{0.282} \qquad (SE = 0.303) \qquad (18)$$
$$\qquad\qquad (0.035) \quad (0.052)$$

$$P/D^2 = K(1/D)^{0.814}(F/D)^{0.215}(L/D)^{0.123} \qquad (SE = 0.302) \qquad (19)$$
$$\qquad\qquad (0.037) \quad (0.067) \quad (0.076)$$

Equation (17) contains the factor $(1/D)^{0.939}$ to take account of the effect of size on PL strength. Equation (18) contains also the shape effect $(F/D)^{0.282}$. Equation (19) takes account of two shape effects. The decreasing trend of c_1 (0.939 to 0.814) is consistent with Eq. (11). SE can be reduced at most to a minimum level that represents the random variability in the data, the variability that remains after the effects of all the significant factors have been accounted for. Both c_1 and SE appear to have reached stable (minimum) values in the three-variable model, Eq. (19), which is therefore taken to be the most accurate representation of the test data.

The number of significant parameters that can be determined from any set of experimental data is limited by the number of parameters that were varied by significant amounts in the tests. For the present PL test data, tests of a single rock type are sufficient to determine only one significant dimension parameter, if all the specimens had the same orientation with respect to the load direction (Table 4). Data sets that contain more than one rock type or more than one test orientation are sufficient to determine two significant dimension parameters (Table 6). The solutions for all of the three-dimension-variable model categories *R, A, B, L, M,* and *S* of Table 7 are analyses of data sets for all-orientations-pooled or all-rock-types-pooled; most of these solutions indicate one or more parameters to be nonsignificant — they fail to meet the criterion that a *c* value be more than twice its standard error; in effect such *c* values are indeterminate. Consequently, such solutions in many instances exhibit "wild" *c* values, and hence the *c*-value ranges of Table 7 are inflated estimates, although they may reflect the robustness of the models relative to each other, the degree to which they may be sensitive to imperfections in the structure of the data. The *P* models of Table 7 do (barely) provide significant estimates for three dimension variables, having been derived from more than one rock type tested at more than one specimen orientation, such that the important parameters *D, F/D,* and *L/D* of Eq. (19) varied over significant ranges, summarized in Table 8.

In Tables 4—7, *D* consistently outperforms *H* as a predictor of *P*, with respect to consistency and goodness of fit. Thus, a testing apparatus or procedure does not require measurement of the final distance between load points, except as a check on behavior. Excessive penetration of the load points during a test suggests that the specimen does not exhibit brittle behavior and therefore that the test should be rejected as not valid.

Looking back over Tables 4—7 one can appreciate the difficulties in attempting to devise a meaningful model from too small a data base — for

Table 8. Ranges and means of parameters in Eqs. (17) — (19), by test category

	Iron-formation		Metadiabase			Basalt	
Load parallel to	*L*	*M*	*L*	*M*	*S*	*M*	*S*
Number of tests	11	34	7	44	80	14	167
Maximum *D*, mm	244	249	234	246	229	234	201
Minimum *D*, mm	71	41	56	38	15	46	15
Mean log *D*	4.76	4.39	4.80	4.66	3.92	4.74	4.24
Std dev log *D*	0.425	0.534	0.540	0.511	0.635	0.441	0.542
Maximum *F/D*	1.17	2.04	1.02	1.87	5.50	1.34	8.29
Minimum *F/D*	0.64	0.66	0.45	0.59	1.05	0.56	1.08
Mean log *F/D*	−0.162	0.091	−0.225	0.056	0.792	−0.080	0.860
Std dev log *F/D*	0.182	0.216	0.281	0.241	0.409	0.262	0.414
Maximum *L/D*	1.00	1.80	1.00	2.33	8.33	2.39	8.14
Minimum *L/D*	1.00	1.04	1.00	1.01	1.30	1.05	1.40
Mean log *L/D*	0	0.267	0	0.294	1.01	0.429	1.10
Std dev log *L/D*	0	0.147	0	0.183	0.417	0.276	0.382

examples, failing to measure at least three dimensions on the test fragments or testing only a single specimen orientation with respect to load. Even so, the present data are none too numerous. Some extreme results obtained from the *LR*- and *MB*-category models, Table 4, suggest that a minimum of 30 tests in any category should be available for analysis.

Analysis of Residuals

Examination of the residuals provides additional insights. In Fig. 8 are plotted residual vs. estimated log P/D^2 for each rock type, including only the data used to establish Eq. (19), namely, both platens of cone shape and fracture surface deviating $<7.5°$ from a line through the load points, and excluding the 7 outliers. Residual = (Observed value of log P/D^2) − (Value of log P/D^2 calculated from the fitted Eq. (19)). If all the test data were an exact fit to the model, the residuals would plot on the horizontal line Residual = 0 for all values of estimated log P/D^2. For all three rocks and for any test orientation, the trend of the scatter is not noticeably greater or smaller, more negative or more positive, over the range of the abscissa values, which implies over-all adequate fit to the data by the form of Eq. (19), expressed as a product of powers, and the analysis of its logarithmic transformation.

Bedding-plane fissility of the iron-formation parallel to its color banding exhibited hardly any influence on its strength behavior, which can be attributed to recementing of the rock during geologic metamorphism. Only 7 of the 58 specimens fractured parallel to the banding; two of these (*L*-axis tests) were excluded from the regressions because their fracture surfaces deviated $>7.5°$ from a line through the load points. Of the other five (mean residual = −0.18), three were *L*-axis tests of which two showed planar fracture surfaces, the only two of the 58 to do so.

The effects of fracture-angle deviation and of flat-surface platens, for tests that were excluded from the tabled solutions, are exhibited by the summary, Table 9, of their residuals with respect to estimates given by Eq. (19). Although none of the mean values differs statistically from zero, the trends are consistent: (i) Increasing deviation of the fracture surface from a line through the load points tends to produce below-average indicated strengths, and (ii) flat platens tend to produce above-average strengths. Testing with one flat platen and one cone appears to raise the indicated strength by 11.6% ($e^{0.11} = 1.116$).

Table 9. Summary of residuals-fracture angles and flat platens

Category	*n*	Mean	Std dev
Fracture surface deviating 7.5°—17.5°	18	−0.26	0.47
Fracture surface deviating 17.5°—47.5°	29	−0.37	0.54
One flat platen and one cone platen	81	0.11	0.39
Two flat platens	4	0.55	0.29

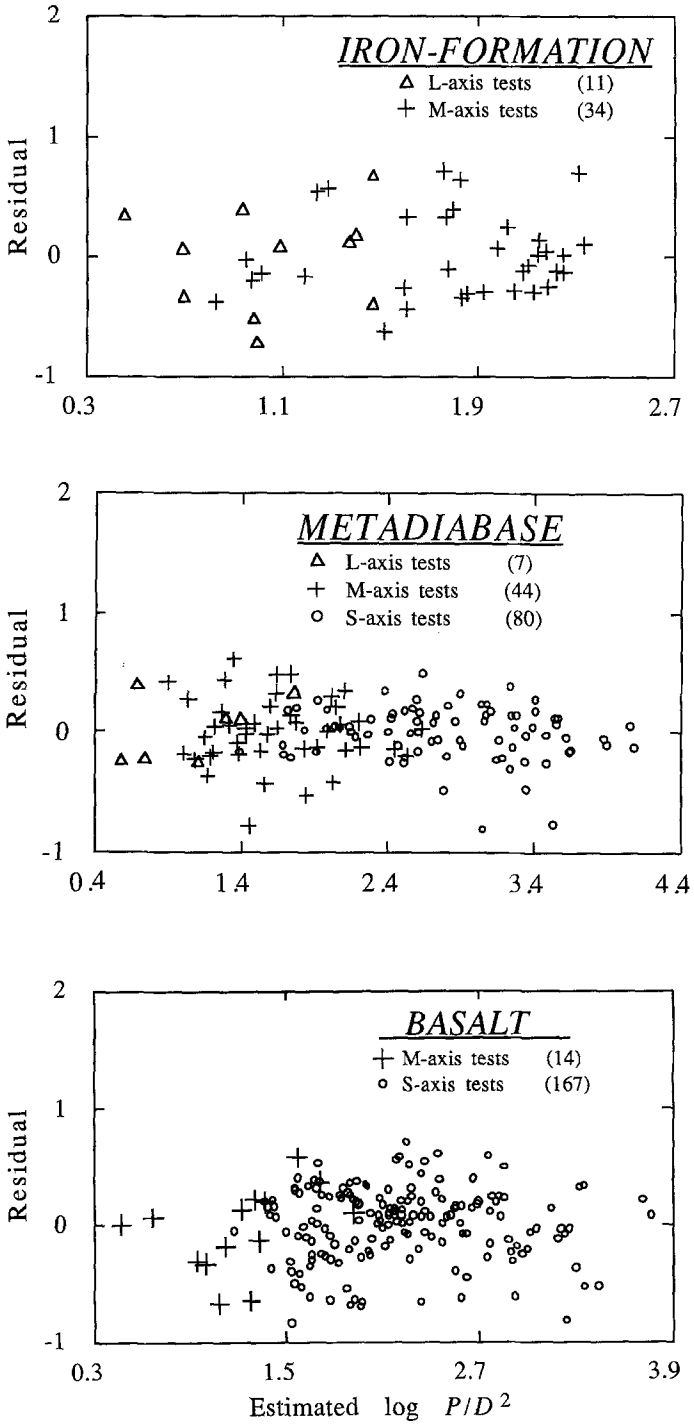

Fig. 8. Point load tests, residuals with respect to Eq. (19)

7. Concluding Comments

PL test measurements were analyzed by multilinear regression analysis to obtain leastsquares estimates of the model parameters, considering power functions of all possible combinations of one, two, or three of the dimension parameters *L, M, S, D, H, F, G, J, U, W, X, Y,* and *V.* Models were compared for efficiency and validity using as objective criteria the goodness of fit to the data, the consistency of the *c* values for the three specimen orientations and the three rock types, and the interactions between the dimension variables and the category variables, orientation and rock type.

In seeking the best estimates of the parameters, the authors necessarily set aside test results that might possibly be influenced by the fracture-angle deviation or the use of a flat-surface platen. For practical, routine testing, however, especially if time is pressing or if available test results are few, one may opt to retain results for which the fracture-angle deviation is as great as 15°, and utilize a flat-surface platen if persistent difficulties are experienced with specimens slipping out from between the load points, *provided that* such data are properly flagged to indicate the deviations from ideal conditions. The present data suggest that these effects are not likely to be substantial.

Rock strength test results depend on specimen size, the influence of which varies with the rock material. A meaningful rock strength determination can be achieved only by testing specimens of varying sizes and calculating therefrom the value of the size-effect exponent, c_1. The smaller the value of the size-effect exponent, especially if $c_1 < 0.1$, the greater must be the range of sizes tested, if the size effect is to be detectable in the data.

In unconfined compression metadiabase exhibited a size-effect exponent $c_1 = 0.39$, much greater than the $c_1 = 0.10$ for basalt, whereas in "tension" by DC tests, little difference was found between the two rocks, $c_1 = 0.22 - 0.32$ for metadiabase vs. $c_1 = 0.29$ for basalt. The c_1 indicated by the DC tests of basalt may have been influenced by the slightly nonstandard method of loading the specimens. In the PL test of irregular fragments, $c_1 \cong 0.81$ for the three crystalline rocks tested, despite the variability as to their c_1 values found in the UC and DC test modes. The PL strength of an irregular fragment is found to be a function of at least one shape ratio, in addition to the size effect.

Listed in Table 10 are the "average" strengths of the three rocks, estimated by Eqs. (4), (5), (8), (9), and (19) for specimens of $D = 50$ mm. The PL test results are calculated from the logarithmic form of Eq. (19), using the mean values found for log *F/D* and log *L/D* in the test specimens, corresponding to the appropriate orientation and rock type (given in Table 8). The *S*-axis PL strength values are close to those of the DC tests. The ratios among PL strengths, *S*-axis tests to *M*-axis tests to *L*-axis tests, are larger than one might expect, because the corresponding specimen dimensions are necessarily quite different, given that the three orientations are compared at $D = 50$ mm.

Table 10. Summary of rock strength determinations, $D = 50$ mm

	Iron-formation	Metadiabase	Basalt
UC tests, MPa	—	182.8	175.2
DC tests, MPA	—	16.92	11.84
PL tests, L-axis, MPa	5.72	6.08	—
PL tests, M-axis, MPa	8.84	9.49	6.54
PL tests, S-axis, MPa	—	16.76	11.99

Acknowledgements

These analyses are based on tests performed by the junior author and submitted as a project report in partial fulfillment of the requirements for the M. S. degree in Mining Engineering at Michigan Technological University. Operating staff of the Tilden Mine, Cleveland Cliffs Iron Company, especially Chief Engineer Terry Lambert, provided assistance in collecting the test samples of iron-formation and metadiabase. B. H. Thomas, Research Assistant at the MTU Experimental Mine, drilled and blasted to create the basalt rock samples. M. A. LaCourt, MTU Training Specialist, was instrumental in preparing the UC and DC test specimens and instructing in the use of the load frame and recording system.

References

Broch, E., Franklin, J. A. (1972): The point-load strength test. Int. J. Rock Mech. Min. Sci. 9, 669—697.

Draper, N. R., Smith, H. (1981): Applied regression analysis. Second edn. J. Wiley, New York, 241.

Fannon, T. A. (1989): The effect of size on rock strength determined by point load tests on irregular shaped rock fragments, uniaxial compression tests, and Brazil tests. Project Report submitted in partial fulfillment of the requirements for M. S. degree in Mining Engineering, Michigan Technological University, Houghton, Michigan.

ISRM Commission on Standardization of Laboratory and Field Tests (1972): Suggested methods for determining the uniaxial compressive strength of rock materials and the point load strength index. ISRM, Lisbon.

ISRM Commission on Testing Methods (1985): Suggested method for determining point load strength (revised). Int. J. Rock Mech. Min.Sci. Geomech. Abstr. 22, 51—60.

Panek, L. A. (1981): Estimating mine pillar strength from compression tests. Trans. AIME, 268, 1749—1761, and Discussion 272, 2005—2009.

Protodyakonov, M. M., Voblikov, V. S. (1957): Determining the strength of rock on samples of an irregular shape. Ugol 32 (4).

Villar, J. W., Dawe, G. A. (1985): The Tilden Mine — A new processing technique for iron ore. Mining Congress Journal 61 (10), 40—48.

Author's address: Dr. Louis A. Panek, 8 Hillside Drive, Denver, CO 80215, U. S. A.